

# Novel experimental methods to characterize the mechanical properties of the aorta

Brooks Lane<sup>a</sup>, Selda Sherifova<sup>b</sup>, Víctor Acosta Santamaría<sup>a</sup>, Jérôme Molimard<sup>a</sup>,  
Gerhard A. Holzapfel<sup>b,c</sup>, and Stéphane Avril<sup>a,b</sup>

<sup>a</sup>Mines Saint-Etienne, Université Jean Monnet, Université de Lyon, INSERM, U 1059 SAINBIOSE, Saint-Étienne, France, <sup>b</sup>Institute of Biomechanics, Graz University of Technology, Graz, Austria, <sup>c</sup>Department of Structural Engineering, Norwegian University of Science and Technology (NTNU), Trondheim, Norway

## Abbreviations

<b>3D</b>	three-dimensional
<b>CCD</b>	charge-coupled device
<b>CT</b>	computed tomography
<b>DIC</b>	digital image correlation
<b>DVC</b>	digital volume correlation
<b>FOV</b>	field of view
<b>LED</b>	light-emitting diode
<b>MRI</b>	magnetic resonance imaging
<b>OCT</b>	optical coherence tomography

## 1 Introduction

Experiments are necessary to study, understand, model, and further predict the mechanical alterations caused by structural and functional changes in the pathological aorta. In clinical follow-up, several noninvasive in vivo measurements can be performed to examine arterial stiffness and distensibility, arterial pressure, intima-media thickness, and arterial diameter. Arterial stiffness has received particular attention in recent years because it can serve as a prognostic biomarker that represents changes in the arterial wall and measures the cumulative influence of cardiovascular risk factors over time (Laurent et al., 2006). Carotid-femoral pulse wave velocity and pulse transit time provide information on structural stiffness, and the effectiveness of pulse wave velocity in clinical follow-up of patients has been shown in various populations (Laurent et al., 2016; Townsend et al., 2015). However, pulse wave velocity as a mechanical parameter does not consider the complexity of the mechanical properties of arteries. The aorta exhibits highly nonlinear and anisotropic mechanical behavior, and different techniques that have been developed to characterize the incremental elastic modulus in vivo and reveal only a small part of the overall mechanical behavior of the arterial wall. Furthermore, these methods are insufficient to model the response of the aortic wall to supraphysiological loads such as those applied

by a stent graft (Perrin et al., 2015a, b, 2016) or to determine the strength of the tissue to evaluate the risks of aneurysm rupture or dissections (Gasser et al., 2010; Vorp, 2007).

More comprehensive characterizations of the arterial wall, e.g., from the stress-free state to failure under different combinations of multiaxial loadings, can only be carried out in vitro on excised specimens. Due to the difficulties in obtaining intact and fresh human tissue, numerous in vitro mechanical tests have been carried out on tissues derived from animal models attempting to reproduce human pathologies, with mice models being the most popular in vascular biology (Fung, 1967, 2013; Humphrey, 2013).

In this chapter, we first review the experiments conducted over more than five decades that have enabled the development of theoretical and numerical models that are widely used in the community of vascular biomechanics (Holzapfel et al., 2000; Humphrey, 2013). We then discuss the significance of regional variations in the material properties of the aorta and review the studies using full-field measurements to assess these variations. Finally, we point out the potential of optical coherence tomography (OCT), which is widely used medically in ophthalmology, dermatology, and more recently, for some cardiovascular investigations, to quantify three-dimensional (3D) local strains in the aorta.

---

## 2 Conventional experimental methods

### 2.1 Uniaxial tests

Given the difficulty of collecting intact pathological arteries, the simplest mechanical test that can be performed at tissue scale and one of the most commonly used is the uniaxial test. The uniaxial test measures the force exerted on a rectangular test piece in response to the elongation imposed on it (uniaxial extension) or vice versa (uniaxial tension, which implies a force-controlled test instead of a displacement-controlled test).

The axial stretch is usually measured through the displacements of the tensile machine jaws, assuming a nearly homogeneous deformation in the center of the sample, as observed in the tests. It should be noted that this stretch, together with the transverse stretch, can also be derived more accurately through video-extensometer measurements between markers drawn on the sample (García-Herrera et al., 2012), using the incompressibility assumption to derive the through-thickness stretch. The engineering stress is derived as the recorded force divided by the initial cross-sectional area.

Rectangular strips can be cut from the excised aortic segment with the circumferential or longitudinal direction as the main axis of loading. In addition to stiffness of the material, the anisotropy of the mechanical response can also be evaluated (O'Leary et al., 2014; Pierce et al., 2015; Sassani et al., 2015; Teng et al., 2015; Vorp et al., 1996). In addition, one can obtain failure properties with the dog-bone shaped samples, e.g., stress and strain at rupture and other material properties of the tissue (Khanafar et al., 2011). It is more convenient to test samples to failure in uniaxial tests, due in large part to the availability of test setups. These tissue characterization tests have been applied to study numerous aortic pathologies (Humphrey, 2013), including aortic aneurysms, see, e.g., Sherifova and Holzapfel (2019) and the references contained therein.

Another simple mechanical test that can be performed on aortic tissues is the ring-tensile test, which is particularly suited to the naturally cylindrical shape of the arteries. Two hooks are inserted into an arterial ring and then pulled apart. The force exerted on the ring is measured while it is elongated.

These tests, used in pharmacology, are also useful to determine the active mechanical properties associated with the contraction of vascular smooth muscle cells in response to vasoconstrictor agents (Cox, 1983) in the presence or absence of an “intact” endothelium. Although ring tests are very popular for these pharmacological studies, they generate heterogeneous strain and stress fields in the ring near the hooks, which has some disadvantages for characterizing the stress-strain behavior. Recently, Haslach et al. (2018) and FitzGibbon and McGarry (2021) used the ring test to robustly and repeatedly produce mode II crack initiation and propagation in aortic rings. In fact, the majority of arterial fracture experiments rely on the mode I peel test (Sommer et al., 2008; Witzenburg et al., 2017) or lap shear tests for mode II fracture (Sommer et al., 2016; Witzenburg et al., 2017). However, lap shear testing produces a mixed mode, while ring testing solves this problem (FitzGibbon and McGarry, 2021).

Uniaxial tests on the aorta have rarely been achieved in the radial direction (radial tension). Poker-chip shape samples were cut with a circular punch and glued between two plates with a cyanoacrylate adhesive (Kumar and Lopez-Pamies, 2021; Nolan and McGarry, 2016; Sommer et al., 2008). This allowed the radial strength or even the compressibility modulus of the aorta to be characterized, but this test remains very difficult to evaluate as it violates the Saint-Venant’s principle (stress distribution is not uniform) due to the very low aspect ratio.

In summary, numerous uniaxial tests have been performed on aortas as the simplest test protocols that provide access to information that cannot be obtained *in vivo*, such as the individual mechanical behavior of the different layers of the wall (intima, media, and adventitia) and their failure properties. However, uniaxial tests cannot produce the complex *in vivo* loading conditions that can be better approximated by multiaxial testing setups.

## 2.2 Multiaxial tests

Multiaxial tests are always preferred as the aorta is subject to a complex loading state *in vivo*, and these tests provide a much broader coverage of the deformation state, which is particularly helpful to determine best-fit values of material parameters for a stored-energy function. Examples of such multiaxial tests include, but are not limited to, planar biaxial extension, bulge inflation, and inflation extension, discussed briefly further.

To better characterize the mechanical state of aortic tissue *in vivo*, one can perform planar biaxial tensile tests, in which a square sample is simultaneously loaded in two orthogonal directions corresponding with the material axes in the circumferential direction  $\theta$  and the longitudinal direction  $L$ . Samples are mounted in a variation of biaxial arrangements originally proposed by Sacks and Sun (2003), in which usually evenly spaced barbless hooks are anchored to Kevlar suture lines on the sides of the sample to provide uniform strain fields in the center of the sample and to avoid edge effects. Typically, one performs multiratio cyclic stretch protocols—including equi-biaxial stretch, proportional stretch, and strip biaxial stretch—so that the obtained dataset covers a variety of loading conditions to which the artery may be exposed *in vivo*. Noting the preferred stretches (circumferential, axial) by  $(\lambda_\theta, \lambda_L)$ , equi-biaxial stretching requires  $\lambda_\theta = \lambda_L$ , proportional stretching requires  $\lambda_\theta = \beta \lambda_L$ , where  $\beta$  typically takes values from 0.3 to 1.6, and strip-biaxial stretching includes  $\lambda_\theta > 1$  for different fixed values of  $\lambda_L$  and  $\lambda_L > 1$  for different fixed values of  $\lambda_\theta$ .

Despite its advantages over uniaxial testing, planar biaxial testing is not well suited for strength assessment due to mounting techniques and the square shape of the specimen, which usually prevents specimen failure in the gage area. Bulge inflation tests, which also mimic the loading conditions that

aneurysms experience, are better suited for failure analysis. Dynamic and quasi-static bulge inflations were performed on healthy descending aortas 40 years ago (Mohan and Melvin, 1983), where the authors reported that aortic tissue failure always occurs with a tear in the circumferential direction, similar to healthy porcine aortic tissue (Marra et al., 2006). More recently, Kim et al. (2012), Romo et al. (2014), and Sugita et al. (2012) performed such inflation tests to assess the equi-biaxial failure properties of the human ascending aorta under healthy and aneurysmal conditions. Bulge-inflation tests alone can be useful to assess possible anisotropy, but require advanced inverse approaches to determine the best-fit parameters in a strain-energy function, since the coverage of the  $(\lambda_\theta, \lambda_L)$  space is limited to the combination of several positions together (Davis et al., 2015).

Given the complexity of its structure and its material heterogeneity, the mechanical properties determined at tissue level are not sufficient to characterize the overall behavior of the aorta. Extension-inflation tests can be used to analyze the mechanical behavior at the level of the vascular structure. These more closely resemble the loading conditions encountered in vivo and preserve the integrity of the aorta and its tubular structure. They typically consist of longitudinally stretching the artery until it reaches an extension close to the in vivo conditions and then pressurizing it to physiological pressure levels. Alternatively, simpler closed-end, free-extension conditions may be applied. From this, the pressure-volume or pressure-diameter relationships and the corresponding longitudinal force values can be determined (Gleason et al., 2004). These relationships can then be used to develop models of mechanical behavior, particularly in the hyperelastic case (Ferruzzi et al., 2011). However, extending the samples to their in vivo extension levels requires a priori knowledge of the in vivo prestretch, which is typically not available, particularly for human arteries (van Loon et al., 1977).

Nevertheless, the extension-inflation tests show a salient feature of the arteries: if the applied axial prestretches are smaller or larger than the optimal (energetically favorable) prestretch, the axial reaction force decreases or increases, respectively, with increasing pressure in the physiological range (Schulze-Bauer et al., 2003). However, if the applied axial prestretch is equal to the optimal prestretch, the axial reaction force during pressurization will remain constant over normal pressure ranges, i.e., the artery does not perform axial work with changes in blood pressure during this axial stretch (Schulze-Bauer et al., 2003). For arteries that are axially compressed rather than extended in vivo (Kamenskiy et al., 2016; Langewouters et al., 1984; Schulze-Bauer et al., 2003), the determination of optimal axial stretch by extension-inflation tests becomes difficult because the artery would buckle under compression (Schulze-Bauer et al., 2003).

Note that the tension inflation test has also become the standard test for mice aortas (Bellini et al., 2017). Mice have emerged as the preferred animal models in modern cardiovascular research for many reasons, including their short gestational period ( $\sim 20$  days) and developmental period ( $\sim 56$  postnatal days to biomechanically mature arteries), the wide availability of genetically modified mice, the ease of surgical and pharmacological manipulation, rapid aging (within 2 years), and of course, the availability of countless antibodies for biological assays (Bellini et al., 2017).

A common limitation to most of the techniques discussed earlier is the assumption of uniform stress and strain distributions when samples are subjected to these loading scenarios, leading to the assumption of uniform material properties. The existence and potential importance of nonuniform properties are supported by advances in vascular mechanobiology (Humphrey, 2008), which imply that cells should be expected to remodel and adapt to local variations in loading, leading to regional variations in material properties. This limitation of uniformity does not result from computational or theoretical limitations, but rather from the lack of more complex experimental setups required to quantify the local variations in material properties.

## 3 Full-field optical measurements

### 3.1 Introduction

Experimental setups that couple mechanical testing with live imaging or microscopy have been developed to elucidate the microstructural mechanisms behind the nonlinear character of the response (Avril et al., 2010; Duprey et al., 2016; Genovese, 2009; Genovese et al., 2012; Kim and Baek, 2011; Romo et al., 2014; Sutton et al., 2008; Zhang et al., 2002). In fact, recent studies have shown that centimeter-sized aortic specimens, a typical size used in the aforementioned mechanical tests, exhibit a significant level of heterogeneity (Davis et al., 2015, 2016). If the material is not sufficiently homogeneous, e.g., in aortic aneurysms (Avril et al., 2010; Davis et al., 2015, 2016), those tests no longer produce a uniform stress field in the central region of the specimens. Therefore, the macroscopic stresses and strains, which are homogenized values, may not sufficiently approximate the local values, especially at the sites of abrupt microstructural changes, such as calcification or fatty deposits of different sizes. Motivated by the need to characterize local conditions, our laboratory and others have developed methods that can be used to obtain submillimeter-resolution strain fields to characterize the regional variations in tissue mechanical properties (Avril et al., 2010; Davis et al., 2015, 2016).

### 3.2 Digital image correlation

Digital image correlation (DIC) is a noncontact method that can be used to determine the complete, full-field surface displacements and strains for general material systems (Palanca et al., 2016). The method was developed by Sutton and coworkers at the University of South Carolina in the early 1980s (Sutton et al., 1983) and further extended to 3D (stereoDIC) measurements (Sutton et al., 2009). The procedure has found a variety of applications for both 2D and 3D deformation measurements on the macroscale.

The mechanical test setups are typically coupled to a number of CCD cameras, at least two for a stereo-DIC measurement (Fig. 1). Lenses of focal length of 35 mm enable a field of view (FOV) of about  $40 \times 40 \text{ mm}^2$  at a working distance of 300 mm with a 1" type CCD array (size:  $13.2 \times 8.8 \text{ mm}^2$ ). The method can achieve spatial resolution in the order of 1/100th of the FOV for the strain measurements (Reu et al., 2015). Extension tubes may also be used to increase the magnification of the lens and hence, the spatial resolution (Genovese et al., 2021). A  $1 \times 1 \text{ mm}^2$  area (typical for a test of a mouse aorta) can be sampled with a spatial resolution on the order of  $10 \mu\text{m}$ . Thus, biomechanical variations occurring at spatial dimensions of around  $10 \mu\text{m}$  can be resolved within the imaged range of  $1 \times 1 \text{ mm}^2$ .

The noncontact nature of DIC offers a major benefit to soft tissues by minimizing the effects of amplification and/or modification of the material response. Furthermore, when applied as a full-field measurement technique, it enables to delineate the local variations in deformation and enables the comparisons with the averaged global deformations, which is crucial when studying inhomogeneous materials such as vascular tissues (Davis et al., 2015; Genovese et al., 2012; Romo et al., 2014). Another advantage is that it can be applied to specimens with any surface shape (curved or planar) and offers the possibility to make accurate measurements on cylindrical structures such as blood vessels. It can be used to measure strains on specimens subjected to out-of-plane bending or twisting, which has been reported for aortas (Weiss et al., 2020). Last but not least, the technique can achieve a point-to-point

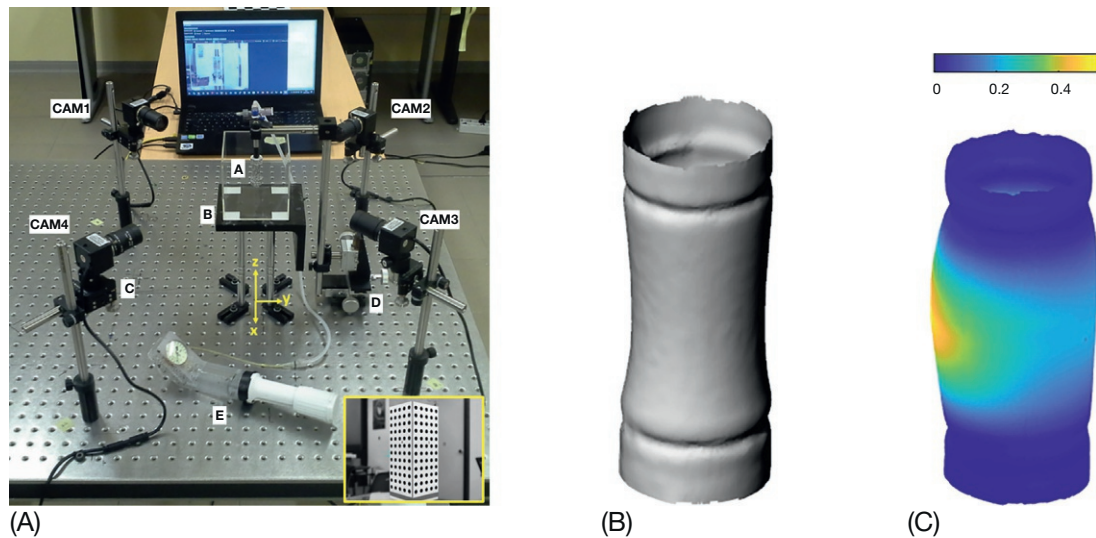


FIG. 1

(a) Picture of a stereo-DIC setup with four cameras allowing a 360 degrees view of an aortic sample: A = sample, B = square acrylic bath, C = camera mounted on a kinematic stage, D = three-axis stage. (b) Undeformed cylindrical shape of a sample measured with the stereo-DIC setup. (c) Map of the maximum principal strain measured with the stereo-DIC setup.

*Courtesy of Genovese, K., Badel, P., Cavinato, C., Pierrat, B., Bersi, M., Avril, S., Humphrey, J., 2021. Multi-view digital image correlation systems for in vitro testing of arteries from mice to humans. Exp. Mech. 61, 1455–1472.*

strain accuracy of up to 0.001 and a full-field average strain accuracy on the order of  $50 \times 10^{-6}$ , allowing both small and large deformation responses to be studied in a single specimen.

Finally, for biaxial testing, it has become standard with DIC to measure by tracking at least several randomized markers placed on the surface of the vessel and the lengths between the two markers in each direction (Pena et al., 2018). Recently, 3D DIC measurements have been coupled with stretch-controlled biaxial testing (Deplano et al., 2016), and the results showed that 3D DIC allows accurate assessment of displacements while improving the accuracy of stress-strain curves in biaxial testing.

Following the pioneering work by Sutton et al. (2008) and Zhang et al. (2002), full-field planar biaxial tests (Deplano et al., 2016; Pena et al., 2018), full-field bulge inflation (Duprey et al., 2016; Romo et al., 2014), and full-field inflation-extension (Avril et al., 2010; Genovese, 2009; Genovese et al., 2012; Kim and Baek, 2011) were performed using DIC to characterize the mechanical and structural properties of aortic tissues. It has been observed that speckle patterns are easier to paint on the intimal face than on the adventitial surface. It is recommended to create them with a fine-tipped air brush and Indian black ink (Genovese et al., 2011). Particular attention must be paid to the quality of the speckle patterns to get about three dots per correlation window. An LED illumination system ensures homogeneous illumination, and the use of polarization filters can avoid specular reflection on the surface of specimens that can often cause DIC artifacts (Kim et al., 2012).

Images of a painted speckle taken with a conventional camera are not always needed for DIC applications. One can make use of other imaging modalities such as OCT. It allows reaching micrometric scales and has shown rapid development, including recent real-time acquisitions (Yabushita et al., 2002). The technique allows visualization of tissue microstructure at different subsurface levels at high resolution with cross-sectional imaging under near-infrared light (Boppart et al., 1999). It has been applied to characterize soft and hard human tissues such as blood vessels (Yabushita et al., 2002), respiratory tract (Pitris et al., 1998), gastrointestinal tissues (Izatt et al., 1996), and cartilage (Herrmann et al., 1999). It has also been used for biomaterial applications such as dental materials, porous 3D scaffolds for tissue engineering, and hydrogels, among others (Huang et al., 2008; Real et al., 2013; Williamson et al., 2011; Yang et al., 2007). It can be combined with mechanical testing devices to characterize the mechanical response of the aortic tissues through elastography and noncontact optical methods (Rogowska et al., 2004). For example, Di Giuseppe et al. (2021) performed stepwise radial tensile tests on descending thoracic aortas in healthy pigs and on ascending thoracic aortic aneurysms in humans and acquired 3D volumes (i.e., image stack) from a region of interest after each loading step. Maximum intensity projection was applied to the stack to obtain a single representative 2D image for each step, and the images were processed by DIC to obtain displacement and strain fields showing localizations. A major benefit of OCT in DIC applications is that it is label-free, meaning that it relies on random patterns emerging from tissue microstructure rather than requiring an artificial speckle pattern.

### 3.3 From DIC to DVC

Due to the complex anisotropic structure of the aorta and the nonlinearity of the mechanical response, the strain gradients can vary significantly not only at the surface but also through the thickness of the tissue. In this context, a full-field 3D deformation measurement that can penetrate the tissue is required to unravel the nonuniformity. Digital volume correlation (DVC) goes beyond the surface information provided by stereo-DIC methods by using volumetric image data, e.g., 3D image volume consisting of several 2D cross-sectional images. To achieve this, a correct correlation between the reconstructed volumes is required (Gillard et al., 2014; Keyes et al., 2016). This can be achieved with local correlation algorithms (Acosta Santamaría et al., 2018; Fu et al., 2013; Keyes et al., 2016; Liu and Morgan, 2007).

In the next section, we continue with the first reports of combined OCT-DVC on aortic tissues (Acosta Santamaría et al., 2018; Santamaría et al., 2020) before turning to our recent findings on crack propagation.

---

## 4 Applications of OCT-DVC

### 4.1 Uniaxial extension with stepwise stress relaxation

In this section, we summarize our results obtained using OCT-DVC to characterize the aorta in uniaxial extension, which we combined with optical clearing agents (Acosta Santamaría et al., 2018; Santamaría et al., 2020). The experimental setup shown in Fig. 2 consists of an OCT scanner, an immersion load cell with a control panel, and manually operated micrometers to apply controlled displacements

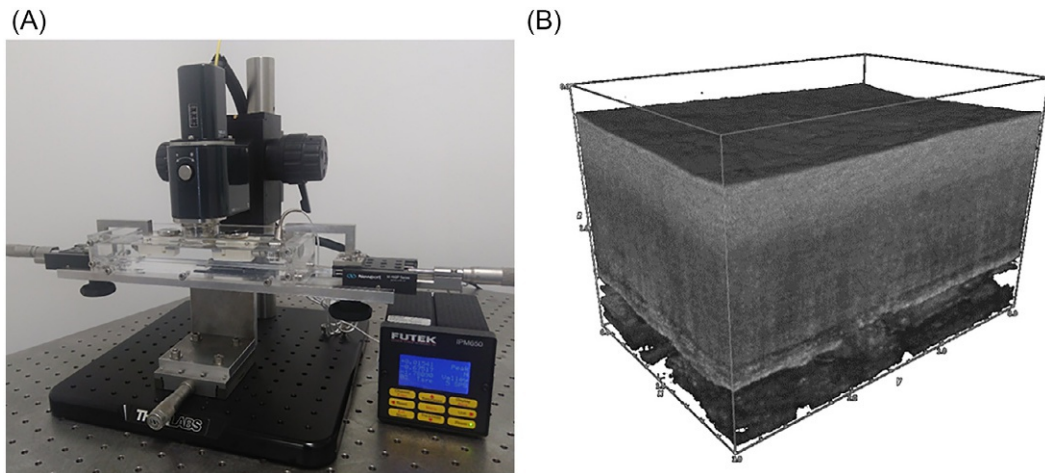


FIG. 2

(A) Experimental overview of quasi-static uniaxial testing of porcine thoracic aorta samples. Samples are held at prescribed stretches during OCT volume acquisition. (B) Typical 3D image sequence acquisition of a full-thickness OCT measurement over an aortic sample.

connected to sample holders placed in a tissue bath container; see [Acosta Santamaría et al. \(2018\)](#) and [Santamaría et al. \(2020\)](#) for detailed specifications.

Circumferentially oriented uniaxial test samples ( $58 \times 10 \text{ mm}^2$ ) prepared from porcine aortas were clamped using grips spaced 35.1 mm apart in the reference configuration. They were preconditioned and then subjected to nine stepwise stress-relaxation ramps. At each loading step, the samples were extended 0.6 mm (0.3 mm from each side) and allowed to relax for 30 min, after which equilibrium was reached. The criterion for complete equilibrium was a relaxation rate  $< 100 \text{ Pa/min}$ . Next, a pre-defined volume was imaged, see [Fig. 2B](#), with a voxel size of  $5 \times 5 \times 2.45 \mu\text{m}^3$  ( $X, Y, Z$ ) and an FOV of  $2 \times 4 \times 2.5 \text{ mm}^3$  ( $X, Y, Z$ ) in 8 min, resulting in a relaxation time of 38 min. At the end of the test, an engineering strain of about 28% was achieved. During the experiments, the OCT illumination tube was in full contact with the immersion bath, and the lens was focused on the luminal surface, i.e., the intima.

The volumes captured with the OCT were saved in TIFF format, imported as a virtual stack into ImageJ software, rescaled, then converted to 8 bits to digitize the intensity levels, and finally, exported as RAW images to be read by DaVis (LaVision) to derive the displacement fields using DVC. To achieve the maximum cross-correlation coefficient (considering the gray-level distributions) when deriving the displacement fields, the subvolume discretization and the multipass approach were used in the software. The detailed discussion of the implemented correlation parameters can be found in our previous work ([Acosta Santamaría et al., 2018](#); [Santamaría et al., 2020](#)). After the 3D displacement fields in each region were obtained, they were approximated by tricubic functions implemented in MatLab ([Santamaría et al., 2020](#)), and the Green-Lagrange strain components were derived ([Fig. 3](#)).

The results show fairly homogeneous depth-resolved strains with minimal shear strains introduced during loading ([Fig. 3](#)). We were able to measure media swelling inducing transverse tensile strain. To the best of our knowledge, this was the first time that such a manifestation of chemoelastic effects in the

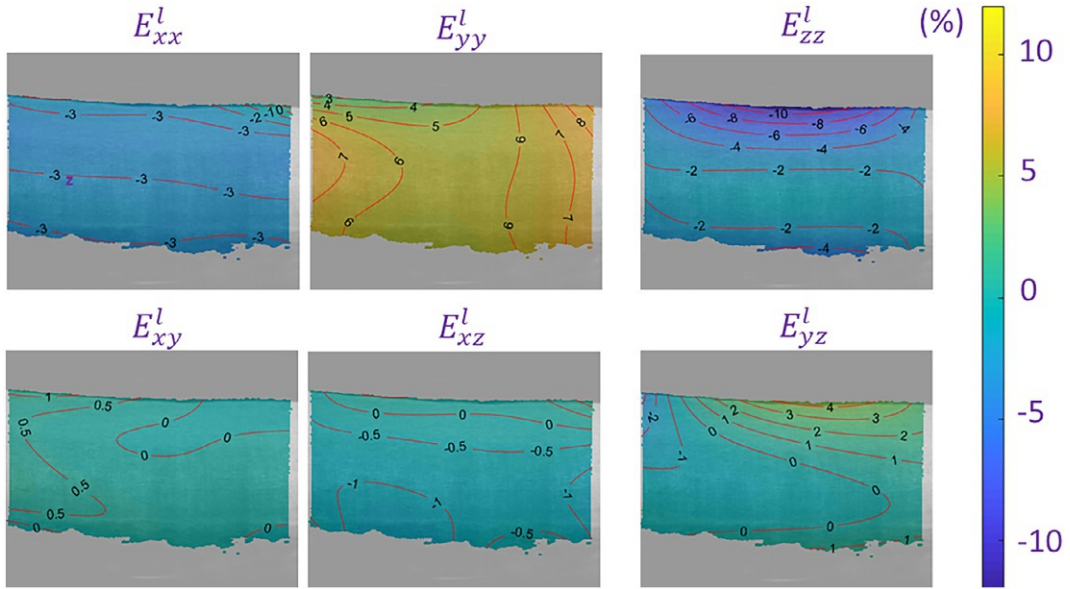


FIG. 3

Local distribution of Green-Lagrange strains  $E_{ij}^E$  obtained using OCT-DVC during an uniaxial extension test at global axial strain  $E_{yy}^E=7\%$  visualized with contour plots (numbers are in %).

aorta could be quantified thanks to the OCT-DVC method (Santamaría et al., 2020). Such effects could play an essential role in arterial mechanobiology in vivo, and we are currently working to characterize them under more physiological conditions, avoiding the effects of the osmotic solution used as a clearing agent (Acosta Santamaría et al., 2018; Santamaría et al., 2020).

## 4.2 Crack propagation

In this section, we report previously unpublished results that highlight the applicability of the OCT-DVC method in quantifying and examining transmural deformations to aid in the characterization of mechanical events before aortic dissection. Aortic dissection is a local pathological event that can be triggered by trauma to the vessel intima or hemorrhage from the *vasa vasorum* resulting in intramural blood pooling (Sherifova and Holzapfel, 2019). Regardless of etiology, the initial insult can propagate and eventually lead to complete vessel failure and rupture, which occurs at the local scale and is often associated with complex processes in failure of interlamellar bridging fibers (Pal et al., 2014).

To reveal complex local intramural deformations in crack propagation in the aortic wall, we applied quasi-static uniaxial loading to circumferentially oriented porcine aortic samples ( $70 \times 10 \text{ mm}^2$ ) with an initial intimal-medial insult. Before the experiment, the samples were immersed in an 80% concentration solution of propylene glycol to optically clear the tissue and improve OCT imaging depth and placed in the experimental apparatus shown in Fig. 2. The samples were clamped with grips 50mm apart in the reference configuration. The arms to which each grip was mounted were moved apart

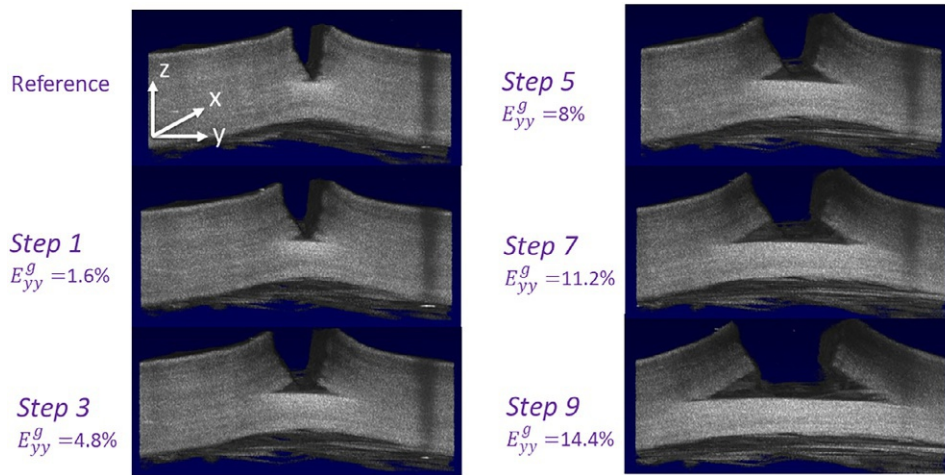


FIG. 4

Sequential volumetric OCT images of the porcine thoracic aorta with medial wall defect and under uniaxial tension showing the maximum global axial strain  $E_{yy}^g$  at different steps.

through micrometers in a stepwise fashion (0.4 mm extension from each side at each step) and held at this stretch for 38 min (30 min relaxation + 8 min during which the OCT volumetric images shown in Fig. 4 were acquired). Nine extension steps were applied, giving a maximum displacement of 3.6 mm on each side and a maximum global axial strain of  $E_{yy}^g = 14\%$ .

The voxel size of OCT images was  $6 \times 6 \times 2.45 \mu\text{m}^3$  ( $X, Y, Z$ ), and the FOV was  $2 \times 3 \times 2.5 \text{mm}^3$  ( $X, Y, Z$ ). The displacement fields were derived using DVC with DaVis. The subvolume discretization and the multipass approach in the software were the same as in our previous work (Acosta Santamaría et al., 2018). After obtaining the 3D displacement fields, they were approximated by tricubic functions implemented in MatLab (Santamaría et al., 2020), and the Green-Lagrange strain components were derived (see Figs. 5 and 6).

Visually, volumetric images at each loading step show that the incremental loading leads to a propagation of the initial insult in the circumferential direction or the direction of the applied extension (Fig. 4). The intact aortic wall below the insult bears all of the tension allied to the vessel, which, interestingly, results in a noticeable change in the optical reflectance of the aortic wall observed as increased signal intensity (whitening) of the intact portion of the wall beneath the insult (Fig. 4). This is probably due to a change of optical properties in the tissue due to the large tensile strains occurring in this region.

Green-Lagrange strains demonstrated the complex and heterogeneous intramural strain distribution in the aorta as the initial luminal defect propagates, see Fig. 5. The large local tensile radial strains ( $E_{zz}^l$ ) in Fig. 5 surround the crack tip, which drives the crack in the circumferential direction, most likely due to failure of radially oriented bridging fibers between the elastic lamellae. This experimental setup does not resolve the microfibrils; however, the experimental protocol could be combined with microscopic techniques including multiphoton second harmonic generation or confocal reflectance microscopy to visualize the crack propagation at the fiber level (Lane et al., 2018; Sang et al., 2021). Shear

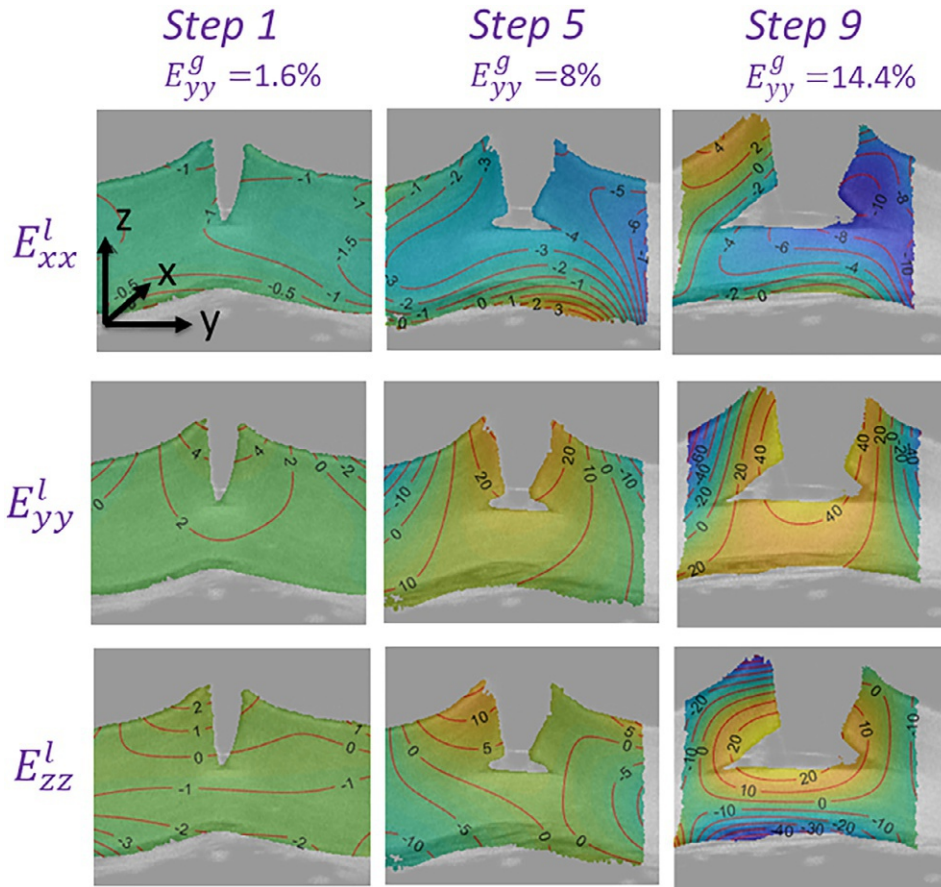


**FIG. 5**

Local distribution of normal Green-Lagrange strain components ( $E^l_{xx}$ ,  $E^l_{yy}$ ,  $E^l_{zz}$ ) obtained with OCT-DVC at three different global strains ( $E^g_{yy}$ ) visualized with contour plots (numbers are in %).

deformations have been proposed to play an essential role in the failure mechanisms under uniaxial loading (Helfenstein-Didier et al., 2018; Sherifova et al., 2019). The quantification of such deformations is depicted for the first time in Fig. 6, where a concentration of local out-of-plane shear strains ( $E^l_{yz}$ ) with nonnegligible values can be seen around the crack tip.

In summary, we have visualized and quantified the intramural strain distributions in the aortic wall under similar, albeit simplified, mechanical conditions as in aortic dissection by combining OCT and DVC. The results underscore the complexity and heterogeneity of the evolving intramural strains upon crack propagation, as evidenced by the significant increase in shear and radial strain magnitudes and their variations.

Despite these achievements, low penetration (0.5mm without clearing agent), time of image acquisition, and possible artifacts caused by local refractive index changes are still limitations of

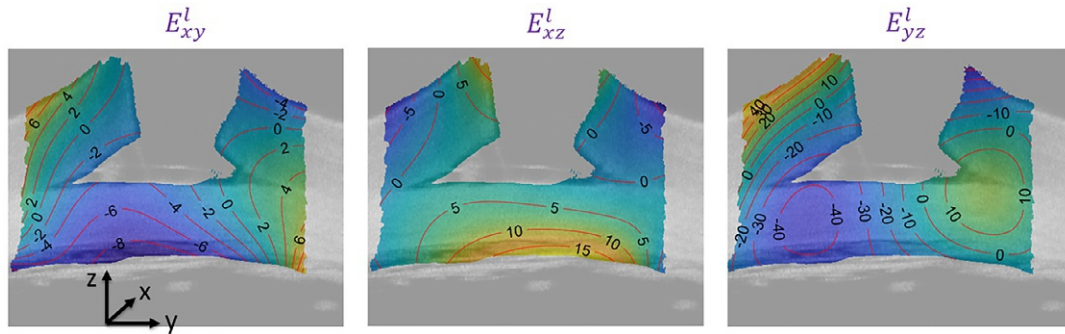


FIG. 6

Local distribution of shear Green-Lagrange strain components ( $E_{xy}^l$ ,  $E_{xz}^l$ ,  $E_{yz}^l$ ) obtained with OCT/DVC at  $E_{yy}^g = 14.4\%$  visualized with contour plots (numbers are in %).

OCT (Liba et al., 2016; Wang, 2002) that must be overcome to popularize the OCT-DVC technique in aorta biomechanics.

## 5 Parameter identification

To identify the material parameters of a model corresponding to a particular aorta, the data from the experiments using full-field methods must be compared with the model by solving an inverse problem. With conventional uniaxial or biaxial tests at the macroscopic scale, the experimental data can be directly translated into terms of stress-strain relationships. Therefore, it is sufficient to optimize the parameters of the constitutive model by minimizing the difference between the experimentally obtained stresses and the stresses computed by the model at the different deformation levels. For this purpose, numerical nonlinear fitting methods such as the least squares method are used.

For more complex tests, however, there are two possibilities. If simplification of hypotheses can be made to generate analytical equations of the mechanical problem, then these equations can be solved numerically through optimization, as explained previously. This is the case, e.g., with the inflation-extension test (Holzapfel et al., 2000). The same approach can also be used in the case of pressure-diameter data obtained in vivo (Masson et al., 2008; Stålhand et al., 2004). If the geometry or loading is too complex to express the analytical equations of the mechanical problem, a finite element model coupled with an inverse method can be used.

Interestingly, a new approach for the in vitro biaxial characterization of human arteries was recently proposed, which allows identification of the material constants in two-fiber and four-fiber family models even in the case of heterogeneous strain and stress distributions in arterial segments (Bersi et al., 2016, 2019; Davis et al., 2015, 2016). We recently applied this approach to the point-by-point characterization of the biomechanical properties of heterogeneous aortic lesions of a murine dissecting aneurysm model with complex morphologies (Bersi et al., 2020). The data were obtained through in vitro extension-inflation experiments coupled with full-field multimodal measurements of wall strain and thickness not only along and around the lesion but also through the wall thickness. More

specifically, to obtain multiaxial mechanical properties, adventitial surface deformations were measured by tracking motions of a speckle pattern using a custom panoramic DIC technique described in [Genovese et al. \(2012\)](#) during deformations throughout the wall and the thrombus, which were derived from OCT-DVC ([Bersi et al., 2020](#)). Results revealed dramatic regional variations in material stiffness and strain energy, reflecting local changes in constituent area fractions obtained from histology, while emphasizing the complexity of lesion morphology and damage within the dissected wall.

---

## 6 Conclusions and future directions

Recent developments in mechanobiology underline the importance of local variations, i.e., nonuniformities of the elastic properties of the arteries, motivating shifting the experimental focus to their quantification. Although we have focused here on our most recent findings using the OCT-DVC modality for such characterizations, alternative methods may include MRI ([Nederveen et al., 2014](#)) or micro-CT ([Brunet et al., 2021](#)), and there are many possible directions for further developments.

To start with, all characterizations reported here were performed under quasi-static conditions. DIC is suitable for both quasi-static and high-speed measurements at rates up to 20,000 frames/s, allowing quantitative measurements to be performed even in the aortas subject to transient environmental and/or loading changes. However, to obtain volumetric data under dynamic loading conditions for the application of DVC, the modalities need to be further improved to reduce imaging time. One must be aware and consider that the application of such methods with sufficient resolution will inevitably lead to tissue-scale data acquisition and processing.

Another critical direction is related to the uncertainty in the data. Given the density of results from new techniques such as OCT-DVC, it is possible to obtain probabilistic distributions of the mechanical response of an aorta. A major challenge of computational soft tissue biomechanics is to transform this a priori probability distribution into a range of uncertainty in the predictions using Bayesian inference ([Zeraatpisheh et al., 2021](#)) or to leverage all these data into data-driven constitutive models, e.g., through deep learning ([Holzapfel et al., 2021](#)).

Last but not least, the aorta is classified as an “elastic” artery that contains large amounts of elastin, in contrast to “muscular” arteries, which are small and highly viscoelastic vessels located at the periphery of the circulatory system. Therefore, experimental efforts have focused on characterizing elastic properties ([Holzapfel et al., 2000](#)), although there is increasing interest in the viscoelastic properties under relaxation or cyclic loading ([Franchini et al., 2021](#); [Kratzberg et al., 2009](#); [Zou and Zhang, 2011](#)). Therefore, the multiscale characterization and modeling of dissipative phenomena are crucial for a better understanding of disease progression and associated catastrophic events and require further experimental investigations.

---

## Acknowledgments

This work was supported by the ERC grants ERC-2014-CoG BIOLOCHANICS, ERC-2014-StG ARTEMIS and the Lead project “Mechanics, Modeling and Simulation of Aortic Dissection” granted by Graz University of Technology, Austria.

## References

- Acosta Santamaría, V.A., Flechas García, M., Molimard, J., Avril, S., 2018. Three-dimensional full-field strain measurements across a whole porcine aorta subjected to tensile loading using optical coherence tomography–digital volume correlation. *Front. Mech. Eng.* 4, 3.
- Avril, S., Badel, P., Duprey, A., 2010. Anisotropic and hyperelastic identification of in vitro human arteries from full-field optical measurements. *J. Biomech.* 43, 2978–2985.
- Bellini, C., Bersi, M., Caulk, A., Ferruzzi, J., Milewicz, D., Ramirez, F., Rifkin, D., Tellides, G., Yanagisawa, H., Humphrey, J., 2017. Comparison of 10 murine models reveals a distinct biomechanical phenotype in thoracic aortic aneurysms. *J. R. Soc. Interface* 14, 20161036.
- Bersi, M.R., Bellini, C., Di Achille, P., Humphrey, J.D., Genovese, K., Avril, S., 2016. Novel methodology for characterizing regional variations in the material properties of murine aortas. *J. Biomech. Eng.* 138.
- Bersi, M.R., Bellini, C., Humphrey, J.D., Avril, S., 2019. Local variations in material and structural properties characterize murine thoracic aortic aneurysm mechanics. *Biomech. Model. Mechanobiol.* 18, 203–218.
- Bersi, M.R., Santamaría, V.A.A., Marback, K., Di Achille, P., Phillips, E.H., Goergen, C.J., Humphrey, J.D., Avril, S., 2020. Multimodality imaging-based characterization of regional material properties in a murine model of aortic dissection. *Sci. Rep.* 10, 1–23.
- Boppart, S.A., Herrmann, J., Pitris, C., Stamper, D.L., Brezinski, M.E., Fujimoto, J.G., 1999. High-resolution optical coherence tomography-guided laser ablation of surgical tissue. *J. Surg. Res.* 82, 275–284.
- Brunet, J., Pierrat, B., Adrien, J., Maire, E., Curt, N., Badel, P., 2021. A novel method for in vitro 3D imaging of dissecting pressurized arterial segments using X-ray microtomography. *Exp. Mech.* 61, 147–157.
- Cox, R.H., 1983. Comparison of arterial wall mechanics using ring and cylindrical segments. *Am. J. Phys. Heart Circ. Phys.* 244, H298–H303.
- Davis, F.M., Luo, Y., Avril, S., Duprey, A., Lu, J., 2015. Pointwise characterization of the elastic properties of planar soft tissues: application to ascending thoracic aneurysms. *Biomech. Model. Mechanobiol.* 14, 967–978.
- Davis, F.M., Luo, Y., Avril, S., Duprey, A., Lu, J., 2016. Local mechanical properties of human ascending thoracic aneurysms. *J. Mech. Behav. Biomed. Mater.* 61, 235–249.
- Deplano, V., Boufi, M., Boiron, O., Guivier-Curien, C., Alimi, Y., Bertrand, E., 2016. Biaxial tensile tests of the porcine ascending aorta. *J. Biomech.* 49, 2031–2037.
- Di Giuseppe, M., Zingales, M., Pasta, S., Avril, S., 2021. In vitro measurement of strain localization preceding dissection of the aortic wall subjected to radial tension. *Exp. Mech.* 61, 119–130.
- Duprey, A., Trabelsi, O., Vola, M., Favre, J.-P., Avril, S., 2016. Biaxial rupture properties of ascending thoracic aortic aneurysms. *Acta Biomater.* 42, 273–285.
- Ferruzzi, J., Vorp, D.A., Humphrey, J., 2011. On constitutive descriptors of the biaxial mechanical behaviour of human abdominal aorta and aneurysms. *J. R. Soc. Interface* 8, 435–450.
- FitzGibbon, B., McGarry, P., 2021. Development of a test method to investigate mode II fracture and dissection of arteries. *Acta Biomater.* 121, 444–460.
- Franchini, G., Breslavsky, I.D., Holzapfel, G.A., Amabili, M., 2021. Viscoelastic characterization of human descending thoracic aortas under cyclic load. *Acta Biomater.* 130, 291–307.
- Fu, J., Pierron, F., Ruiz, P.D., 2013. Elastic stiffness characterization using three-dimensional full-field deformation obtained with optical coherence tomography and digital volume correlation. *J. Biomed. Opt.* 18, 121512.
- Fung, Y., 1967. Elasticity of soft tissues in simple elongation. *Am. J. Physiol.-Legacy Content* 213, 1532–1544.
- Fung, Y., 2013. *Biomechanics: Mechanical Properties of Living Tissues*. Springer Science & Business Media.
- García-Herrera, C.M., Celentano, D.J., Cruchaga, M.A., Rojo, F.J., Atenza, J.M., Guinea, G.V., Goicolea, J.M., 2012. Mechanical characterisation of the human thoracic descending aorta: experiments and modelling. *Comput. Meth. Biomech. Biomed. Eng.* 15, 185–193.

- Gasser, T.C., Auer, M., Labruto, F., Swedenborg, J., Roy, J., 2010. Biomechanical rupture risk assessment of abdominal aortic aneurysms: model complexity versus predictability of finite element simulations. *Eur. J. Vasc. Endovasc. Surg.* 40, 176–185.
- Genovese, K., 2009. A video-optical system for time-resolved whole-body measurement on vascular segments. *Opt. Lasers Eng.* 47, 995–1008.
- Genovese, K., Lee, Y., Humphrey, J., 2011. Novel optical system for in vitro quantification of full surface strain fields in small arteries: II. Correction for refraction and illustrative results. *Comput. Meth. Biomech. Biomed. Eng.* 14, 227–237.
- Genovese, K., Collins, M., Lee, Y., Humphrey, J., 2012. Regional finite strains in an angiotensin-II induced mouse model of dissecting abdominal aortic aneurysms. *Cardiovasc. Eng. Technol.* 3, 194–202.
- Genovese, K., Badel, P., Cavinato, C., Pierrat, B., Bersi, M., Avril, S., Humphrey, J., 2021. Multi-view digital image correlation systems for in vitro testing of arteries from mice to humans. *Exp. Mech.* 61, 1455–1472.
- Gillard, F., Boardman, R., Mavrogordato, M., Hollis, D., Sinclair, I., Pierron, F., Browne, M., 2014. The application of digital volume correlation (DVC) to study the microstructural behaviour of trabecular bone during compression. *J. Mech. Behav. Biomed. Mater.* 29, 480–499.
- Gleason, R., Gray, S., Wilson, E., Humphrey, J., 2004. A multiaxial computer-controlled organ culture and biomechanical device for mouse carotid arteries. *J. Biomech. Eng.* 126, 787–795.
- Haslach Jr., H.W., Siddiqui, A., Weerasooriya, A., Nguyen, R., Roshgadol, J., Monforte, N., McMahon, E., 2018. Fracture mechanics of shear crack propagation and dissection in the healthy bovine descending aortic media. *Acta Biomater.* 68, 53–66.
- Helfenstein-Didier, C., Taïnoff, D., Viville, J., Adrien, J., Maire, É., Badel, P., 2018. Tensile rupture of medial arterial tissue studied by X-ray micro-tomography on stained samples. *J. Mech. Behav. Biomed. Mater.* 78, 362–368.
- Herrmann, J.M., Pitris, C., Bouma, B.E., Boppart, S.A., Jesser, C.A., Stamper, D.L., Fujimoto, J.G., Brezinski, M. E., 1999. High resolution imaging of normal and osteoarthritic cartilage with optical coherence tomography. *J. Rheumatol.* 26, 627–635.
- Holzapfel, G.A., Gasser, T.C., Ogden, R.W., 2000. A new constitutive framework for arterial wall mechanics and a comparative study of material models. *J. Elast. Phys. Sci. Solids* 61, 1–48.
- Holzapfel, G.A., Linka, K., Sherifova, S., Cyron, C.J., 2021. Predictive constitutive modelling of arteries by deep learning. *J. R. Soc. Interface* 18, 20210411.
- Huang, Y.-P., Zheng, Y.-P., Wang, S.-Z., Chen, Z.-P., Huang, Q.-H., He, Y.-H., 2008. An optical coherence tomography (OCT)-based air jet indentation system for measuring the mechanical properties of soft tissues. *Meas. Sci. Technol.* 20, 015805.
- Humphrey, J., 2008. Vascular adaptation and mechanical homeostasis at tissue, cellular, and sub-cellular levels. *Cell Biochem. Biophys.* 50, 53–78.
- Humphrey, J.D., 2013. *Cardiovascular Solid Mechanics: Cells, Tissues, and Organs*. Springer Science & Business Media.
- Izatt, J.A., Kulkarni, M.D., Wang, H.-W., Kobayashi, K., Sivak, M.V., 1996. Optical coherence tomography and microscopy in gastrointestinal tissues. *IEEE J. Select. Topics Quant. Electr.* 2, 1017–1028.
- Kamenskiy, A., Seas, A., Bowen, G., Deegan, P., Desyatova, A., Bohlim, N., Poulson, W., MacTaggart, J., 2016. In situ longitudinal pre-stretch in the human femoropopliteal artery. *Acta Biomater.* 32, 231–237.
- Keyes, S.D., Gillard, F., Soper, N., Mavrogordato, M.N., Sinclair, I., Roose, T., 2016. Mapping soil deformation around plant roots using in vivo 4D X-ray computed tomography and digital volume correlation. *J. Biomech.* 49, 1802–1811. <https://doi.org/10.1016/j.jbiomech.2016.04.023>.
- Khanafer, K., Duprey, A., Zainal, M., Schlicht, M., Williams, D., Berguer, R., 2011. Determination of the elastic modulus of ascending thoracic aortic aneurysm at different ranges of pressure using uniaxial tensile testing. *J. Thorac. Cardiovasc. Surg.* 142, 682–686. <https://doi.org/10.1016/J.JTCVS.2010.09.068>.

- Kim, J., Baek, S., 2011. Circumferential variations of mechanical behavior of the porcine thoracic aorta during the inflation test. *J. Biomech.* 44, 1941–1947.
- Kim, J.-H., Avril, S., Duprey, A., Favre, J.-P., 2012. Experimental characterization of rupture in human aortic aneurysms using a full-field measurement technique. *Biomech. Model. Mechanobiol.* 11, 841–853.
- Kratzberg, J.A., Walker, P.J., Rikkers, E., Raghavan, M.L., 2009. The effect of proteolytic treatment on plastic deformation of porcine aortic tissue. *J. Mech. Behav. Biomed. Mater.* 2, 65–72.
- Kumar, A., Lopez-Pamies, O., 2021. The poker-chip experiments of gent and Lindley (1959) explained. *J. Mech. Phys. Solids* 150, 104359.
- Lane, B.A., Harmon, K.A., Goodwin, R.L., Yost, M.J., Shazly, T., Eberth, J.F., 2018. Constitutive modeling of compressible type-I collagen hydrogels. *Med. Eng. Phys.* 53, 39–48.
- Langewouters, G., Wesseling, K., Goedhard, W., 1984. The static elastic properties of 45 human thoracic and 20 abdominal aortas in vitro and the parameters of a new model. *J. Biomech.* 17, 425–435.
- Laurent, S., Cockcroft, J., Van Bortel, L., Boutouyrie, P., Giannattasio, C., Hayoz, D., Pannier, B., Vlachopoulos, C., Wilkinson, I., Struijker-Boudier, H., 2006. Expert consensus document on arterial stiffness: methodological issues and clinical applications. *Eur. Heart J.* 27, 2588–2605.
- Laurent, S., Marais, L., Boutouyrie, P., 2016. The noninvasive assessment of vascular aging. *Can. J. Cardiol.* 32, 669–679.
- Liba, O., SoRelle, E.D., Sen, D., de La Zerda, A., 2016. Contrast-enhanced optical coherence tomography with picomolar sensitivity for functional in vivo imaging. *Sci. Rep.* 6, 1–12.
- Liu, L., Morgan, E.F., 2007. Accuracy and precision of digital volume correlation in quantifying displacements and strains in trabecular bone. *J. Biomech.* 40, 3516–3520. <https://doi.org/10.1016/j.jbiomech.2007.04.019>.
- Marra, S.P., Kennedy, F.E., Kinkaid, J.N., Fillinger, M.F., 2006. Elastic and rupture properties of porcine aortic tissue measured using inflation testing. *Cardiovasc. Eng.* 6, 123–131.
- Masson, I., Boutouyrie, P., Laurent, S., Humphrey, J.D., Zidi, M., 2008. Characterization of arterial wall mechanical behavior and stresses from human clinical data. *J. Biomech.* 41, 2618–2627.
- Mohan, D., Melvin, J.W., 1983. Failure properties of passive human aortic tissue. II—Biaxial tension tests. *J. Biomech.* 16, 31–44.
- Nederveen, A.J., Avril, S., Speelman, L., 2014. MRI strain imaging of the carotid artery: present limitations and future challenges. *J. Biomech.* 47, 824–833.
- Nolan, D., McGarry, J., 2016. On the compressibility of arterial tissue. *Ann. Biomed. Eng.* 44, 993–1007.
- O’Leary, S.A., Healey, D.A., Kavanagh, E.G., Walsh, M.T., McGloughlin, T.M., Doyle, B.J., 2014. The biaxial biomechanical behavior of abdominal aortic aneurysm tissue. *Ann. Biomed. Eng.* 42, 2440–2450.
- Pal, S., Tsamis, A., Pasta, S., D’Amore, A., Gleason, T.G., Vorp, D.A., Maiti, S., 2014. A mechanistic model on the role of “radially-running” collagen fibers on dissection properties of human ascending thoracic aorta. *J. Biomech.* 47, 981–988.
- Palanca, M., Tozzi, G., Cristofolini, L., 2016. The use of digital image correlation in the biomechanical area: a review. *Int. Biomech.* 3, 1–21.
- Pena, J.A., Corral, V., Martinez, M.A., Pena, E., 2018. Over length quantification of the multiaxial mechanical properties of the ascending, descending and abdominal aorta using digital image correlation. *J. Mech. Behav. Biomed. Mater.* 77, 434–445.
- Perrin, D., Badel, P., Orgéas, L., Geindreau, C., Dumenil, A., Albertini, J.-N., Avril, S., 2015a. Patient-specific numerical simulation of stent-graft deployment: validation on three clinical cases. *J. Biomech.* 48, 1868–1875.
- Perrin, D., Demanget, N., Badel, P., Avril, S., Orgéas, L., Geindreau, C., Albertini, J.-N., 2015b. Deployment of stent grafts in curved aneurysmal arteries: toward a predictive numerical tool. *Int. J. Numer. Meth. Biomed. Eng.* 31, e02698.
- Perrin, D., Badel, P., Orgeas, L., Geindreau, C., Rolland du Roscoat, S., Albertini, J.-N., Avril, S., 2016. Patient-specific simulation of endovascular repair surgery with tortuous aneurysms requiring flexible stent-grafts. *J. Mech. Behav. Biomed. Mater.* 63, 86–99.

- Pierce, D.M., Maier, F., Weisbecker, H., Viertler, C., Verbrugge, P., Famaey, N., Fourneau, I., Herijgers, P., Holzapfel, G.A., 2015. Human thoracic and abdominal aortic aneurysmal tissues: damage experiments, statistical analysis and constitutive modeling. *J. Mech. Behav. Biomed. Mater.* 41, 92–107.
- Pitris, C., Brezinski, M.E., Bouma, B.E., Tearney, G.J., Southern, J.F., Fujimoto, J.G., 1998. High resolution imaging of the upper respiratory tract with optical coherence tomography: a feasibility study. *Am. J. Respir. Crit. Care Med.* 157, 1640–1644.
- Real, E., Eguizabal, A., Pontón, A., Díez, M.C., Val-Bernal, J.F., Mayorga, M., Revuelta, J.M., López-Higuera, J.M., Conde, O.M., 2013. Optical coherence tomography assessment of vessel wall degradation in thoracic aortic aneurysms. *J. Biomed. Opt.* 18, 126003.
- Reu, P.L., Sweatt, W., Miller, T., Fleming, D., 2015. Camera system resolution and its influence on digital image correlation. *Exp. Mech.* 55, 9–25.
- Rogowska, J., Patel, N., Fujimoto, J., Brezinski, M., 2004. Optical coherence tomographic elastography technique for measuring deformation and strain of atherosclerotic tissues. *Heart* 90, 556–562.
- Romo, A., Badel, P., Duprey, A., Favre, J.-P., Avril, S., 2014. In vitro analysis of localized aneurysm rupture. *J. Biomech.* 47, 607–616.
- Sacks, M.S., Sun, W., 2003. Multiaxial mechanical behavior of biological materials. *Annu. Rev. Biomed. Eng.* 5, 251–284.
- Sang, C., Kallmes, D., Kadirvel, R., Durka, M., Ding, Y.-H., Dai, D., Watkins, S., Robertson, A., 2021. Adaptive remodeling in the elastase-induced rabbit aneurysms. *Exp. Mech.* 61, 263–283.
- Santamaría, V.A.A., García, M.F., Molimard, J., Avril, S., 2020. Characterization of chemoelastic effects in arteries using digital volume correlation and optical coherence tomography. *Acta Biomater.* 102, 127–137.
- Sassani, S.G., Kakisis, J., Tsangaris, S., Sokolis, D.P., 2015. Layer-dependent wall properties of abdominal aortic aneurysms: experimental study and material characterization. *J. Mech. Behav. Biomed. Mater.* 49, 141–161.
- Schulze-Bauer, C.A., Mörth, C., Holzapfel, G.A., 2003. Passive biaxial mechanical response of aged human iliac arteries. *J. Biomech. Eng.* 125, 395–406.
- Sherifova, S., Holzapfel, G.A., 2019. Biomechanics of aortic wall failure with a focus on dissection and aneurysm: a review. *Acta Biomater.* 99, 1–17.
- Sherifova, S., Sommer, G., Viertler, C., Regitnig, P., Caranasos, T., Smith, M.A., Griffith, B.E., Ogden, R.W., Holzapfel, G.A., 2019. Failure properties and microstructure of healthy and aneurysmatic human thoracic aortas subjected to uniaxial extension with a focus on the media. *Acta Biomater.* 99, 443–456.
- Sommer, G., Gasser, T.C., Regitnig, P., Auer, M., Holzapfel, G.A., 2008. Dissection properties of the human aortic media: an experimental study. *J. Biomech. Eng.* 130, 021007.
- Sommer, G., Sherifova, S., Oberwalder, P.J., Dapunt, O.E., Ursomanno, P.A., DeAnda, A., Griffith, B.E., Holzapfel, G.A., 2016. Mechanical strength of aneurysmatic and dissected human thoracic aortas at different shear loading modes. *J. Biomech.* 49, 2374–2382.
- Stålhand, J., Klarbring, A., Karlsson, M., 2004. Towards in vivo aorta material identification and stress estimation. *Biomech. Model. Mechanobiol.* 2, 169–186.
- Sugita, S., Matsumoto, T., Ohashi, T., Kumagai, K., Akimoto, H., Tabayashi, K., Sato, M., 2012. Evaluation of rupture properties of thoracic aortic aneurysms in a pressure-imposed test for rupture risk estimation. *Cardiovasc. Eng. Technol.* 3, 41–51.
- Sutton, M.A., Wolters, W., Peters, W., Ranson, W., McNeill, S., 1983. Determination of displacements using an improved digital correlation method. *Image Vis. Comput.* 1, 133–139.
- Sutton, M., Ke, X., Lessner, S., Goldbach, M., Yost, M., Zhao, F., Schreier, H., 2008. Strain field measurements on mouse carotid arteries using microscopic three-dimensional digital image correlation. *J. Biomed. Mater. Res. Part A: Off. J. Soc. Biomater. Jpn. Soc. Biomater. Aust. Soc. Biomater. Korean Soc. Biomater.* 84, 178–190.
- Sutton, M.A., Orteu, J.J., Schreier, H., 2009. *Image Correlation for Shape, Motion and Deformation Measurements: Basic Concepts, Theory and Applications.* Springer Science & Business Media.

- Teng, Z., Feng, J., Zhang, Y., Huang, Y., Sutcliffe, M.P., Brown, A.J., Jing, Z., Gillard, J.H., Lu, Q., 2015. Layer- and direction-specific material properties, extreme extensibility and ultimate material strength of human abdominal aorta and aneurysm: a uniaxial extension study. *Ann. Biomed. Eng.* 43, 2745–2759.
- Townsend, R.R., Wilkinson, I.B., Schiffrin, E.L., Avolio, A.P., Chirinos, J.A., Cockcroft, J.R., Heffernan, K.S., Lakatta, E.G., McEniery, C.M., Mitchell, G.F., et al., 2015. Recommendations for improving and standardizing vascular research on arterial stiffness: a scientific statement from the American Heart Association. *Hypertension* 66, 698–722.
- van Loon, P., Klip, W., Bradley, E., 1977. Length–force and volume–pressure relationships of arteries. *Biorheology* 14, 181–201.
- Vorp, D.A., 2007. Biomechanics of abdominal aortic aneurysm. *J. Biomech.* 40, 1887–1902.
- Vorp, D.A., Raghavan, M., Muluk, S.C., Makaroun, M.S., Steed, D.L., Shapiro, R., Webster, M.W., 1996. Wall strength and stiffness of aneurysmal and nonaneurysmal abdominal aorta. *Ann. N. Y. Acad. Sci.* 800, 274–276.
- Wang, R.K., 2002. Tissue clearing as a tool to enhance imaging capability for optical coherence tomography. In: *Coherence Domain Optical Methods in Biomedical Science and Clinical Applications VI. International Society for Optics and Photonics*, pp. 22–25.
- Weiss, D., Cavinato, C., Gray, A., Ramachandra, A.B., Avril, S., Humphrey, J.D., Latorre, M., 2020. Mechanics-driven mechanobiological mechanisms of arterial tortuosity. *Sci. Adv.* 6, eabd3574.
- Williamson, J.P., McLaughlin, R.A., Noffsinger, W.J., James, A.L., Baker, V.A., Curatolo, A., Armstrong, J.J., Regli, A., Shepherd, K.L., Marks, G.B., et al., 2011. Elastic properties of the central airways in obstructive lung diseases measured using anatomical optical coherence tomography. *Am. J. Respir. Crit. Care Med.* 183, 612–619.
- Witzenburg, C.M., Dhume, R.Y., Shah, S.B., Korenczuk, C.E., Wagner, H.P., Alford, P.W., Barocas, V.H., 2017. Failure of the porcine ascending aorta: multidirectional experiments and a unifying microstructural model. *J. Biomech. Eng.* 139, 031005.
- Yabushita, H., Bouma, B.E., Houser, S.L., Aretz, H.T., Jang, I.-K., Schlenkorf, K.H., Kauffman, C.R., Shishkov, M., Kang, D.-H., Halpern, E.F., et al., 2002. Characterization of human atherosclerosis by optical coherence tomography. *Circulation* 106, 1640–1645.
- Yang, Y., Bagnaninchi, P.O., Ahearne, M., Wang, R.K., Liu, K.-K., 2007. A novel optical coherence tomography-based micro-indentation technique for mechanical characterization of hydrogels. *J. R. Soc. Interface* 4, 1169–1173.
- Zeraatpisheh, M., Bordas, S.P., Beex, L.A., 2021. Bayesian model uncertainty quantification for hyperelastic soft tissue models. *Data-Centric Eng.* 2.
- Zhang, D., Eggleton, C.D., Arola, D.D., 2002. Evaluating the mechanical behavior of arterial tissue using digital image correlation. *Exp. Mech.* 42, 409–416.
- Zou, Y., Zhang, Y., 2011. The orthotropic viscoelastic behavior of aortic elastin. *Biomech. Model. Mechanobiol.* 10, 613–625.